

Generalised Polynomial Chaos Based Particle Filter for Orbit Determination

By Yang YANG,^{1),2)} Yanlong BU³⁾

¹⁾SPACE Research Centre, School of Science, RMIT University, Melbourne, Australia

²⁾Space Environment Research Centre, Canberra, Australia

³⁾Beijing Aerospace Control Centre, Beijing, China

(Received June 21st, 2017)

The increased population in space of uncontrollable objects (e.g., space debris) poses severe threats to space assets. In order to avoid collisions with space debris and schedule space missions, the acquisition of highly accurate and reliable state information of these threatening objects is essential. However, due to the sparsity of observations collected by limited sensors on ground, non-Gaussian errors could be introduced into the orbit prediction process without measurement correction. Moreover, uncertain parameters (e.g., the ballistic coefficient, area-to-mass ratio, etc) may also make the non-Gaussianity of orbital dynamics more severe. Both lead to very challenging orbit determination (OD) tasks. The particle filter (PF) is widely used for state estimation of nonlinear systems with non-Gaussian uncertainty based on sequential Monte Carlo simulations (MCS). The generalised polynomial chaos (gPC) theory can also benefit from MCS methods to approximate a dynamic model for uncertainty propagation of model parameters and initial conditions. In this sense, this work integrates the gPC into the traditional bootstrap PF algorithm (gPCPF) for the non-linear and non-Gaussian OD problem. A high area-to-mass ratio object in an inclined geosynchronous Earth orbit is used for validating the efficacy of the proposed gPCPF with simulated ground-based range and range rate measurements. Its performance is compared with extended Kalman filter, unscented Kalman filter (UKF), Gaussian mixture UKF and the bootstrap PF. The results indicate gPCPF outperforms other filters with an uncertain orbital parameter (i.e., the ballistic coefficient) handled.

Key Words: Particle Filter, Generalised Polynomial Chaos, High Area-to-Mass Ratio, Orbit Determination

Nomenclature

x	: Orbital state vector
p	: Orbital parameter vector
z	: Measurement vector
f	: Nonlinear dynamic model
h	: Nonlinear measurement model
v	: Measurement noise
X	: Augmented state vector
ϕ	: The generalised polynomial basis function
ξ	: Multidimensional random variable
α	: Multidimensional index
Φ	: Multivariate basis function
C	: Matrix of gPC coefficients
η	: Standard Gaussian independent random vector
\hat{C}	: Matrix of coefficients of truncated gPC
H	: $M \times N$ Matrix of polynomials
$p(\cdot)$: Probability density function
ω	: Weight
a_{SRP}	: Solar radiation pressure acceleration
B	: Ballistic coefficient

1. Introduction

Due to the large number of resident space objects (RSOs) and the limited number of sensors available to track them, space surveillance is subject to large observation gaps. In addition, the large propagation intervals coupled with nonlinear RSO dynamics result in a highly non-Gaussian probability distribution of the orbital state. Therefore, only estimation techniques that can handle both non-linear and non-Gaussian (NLNG) problem, are suitable for orbit determination (OD) for these RSOs.

The research into the field of online, real-time state estimation based on dynamic models dates back to 1960, when Rudolf E. Kalman developed a minimum-variance estimator, namely the Kalman filter (KF), for linear stochastic systems with assumed Gaussian distributions in his seminal paper.¹⁵⁾ Since then, KF and its variants have been widely used in estimation problems. The extended Kalman filter (EKF) is commonly used for real-time nonlinear estimation by linearising the dynamic and/or measurement equations at each time step via first-order Taylor expansions.²⁴⁾ However it fails when the simple linearisation causes a considerably inaccurate approximation. Thus, some other variants, like the Gaussian higher-order KF (GHKF) that takes second- or even higher- order approximation of the nonlinearity, have been proposed.⁹⁾ Another set of alternatives are sigma point Kalman filters (SPKF), including the unscented Kalman filter,¹⁴⁾ the central difference filter¹²⁾ and the divided difference filter.²¹⁾ SPKFs essentially are sampling-based filters and can yield more accurate results than an EKF or GHKF, especially when accurate initial condition states are not well known.⁷⁾ But SPKFs are often slightly slower than the EKF.

For most general real-world systems, filters that do not rely on the Gaussian assumption have also been investigated. The Gaussian sum Kalman filter, like the Gaussian mixture unscented Kalman filter (GMUKF), is proposed to deal with NLNG problems by approximating the a posterior probability density function (PDF) using a weighted sum of Gaussian PDFs.¹²⁾ A second general approach to NLNG filtering is known as a particle filter (PF), based on sequential Monte Carlo simulation (MCS).¹⁾ PF can provide satisfactory accuracy of the solutions in the NLNG cases but also poses high computational costs.

Obviously filters need to handle uncertainties involved in the

system's dynamics and associated observations so as to obtain optimal estimates. As a useful alternative to statistical methods, the generalised polynomial chaos (gPC) theory is proposed to account for the effects of arbitrary, time-invariant uncertainties associated with model parameters and initial conditions.²⁷⁾ It is an extension of the classical polynomial chaos expansions²⁵⁾ for substituting the stochastic system by an alternative deterministic system with a linear combination of orthogonal basis functions and propagating the associated uncertainties onto the system response without experiencing any constraints of linear dynamics, or Gaussian distributions of the uncertainty sources. The gPC method has been applied in many space applications, e.g., orbit uncertainty propagation.^{13,23)} It also has been integrated with filters for state and parameter estimation.^{3,17,18,28)}

The main idea of this paper is to combine the generalised polynomial chaos (gPC) with PFs (gPCPF) in a hybrid scheme, and compare the gPCPF with the bootstrap PFs in the OD problem with nuisance orbital parameters. To be specific, the gPC is used to propagate the orbital state with an uncertain parameter through the non-linear dynamics. Then a generic PF scheme is implemented for the posterior orbital state and PDF estimation. The basis polynomials of gPC need to be regenerated based on the posterior PDF for the next iteration. Finally, numerical simulations are given for testing the OD performance by the proposed gPCPF algorithm with ground-based observations. Two scenarios are given: one is an inclined geosynchronous Earth orbit (IGSO) following a Keplerian motion and the other one is to assume a high area-to-mass ratio (HAMR) with this IGSO and the solar radiation pressure (SRP) is considered with an uncertain ballistic coefficient. gPCPF filtering performance is compared with extended Kalman filter (EKF) and the bootstrap PF, in terms of state estimation and sensitivity analysis of the parametric uncertainties.

The rest of the paper is organised as follows: Section 2. gives the nonlinear stochastic model of the system with non-Gaussian parametric uncertainty. The mathematical details for the gPC methodology is introduced in Section 3. Section 4. introduces the formulation of particle filters followed by the proposed gPCPF algorithm given in Section 5. Two numerical examples are used to test the performance of gPCPF in Section 5. Section 6. draws the conclusions of this paper and discusses some future work.

2. Problem Formulation

Consider a general continuous-time nonlinear dynamic system with uncertain initial state and parameters and a discrete-time measurement model

$$\dot{\mathbf{x}} = \mathbf{f}(\mathbf{x}, \mathbf{p}, t), \quad (1)$$

$$\mathbf{z}_k = \mathbf{h}(\mathbf{x}_{t_k}) + \mathbf{v}_k, \quad (2)$$

where $\mathbf{x}(t_k)$ denotes the n -dimensional state vector at the time epoch t_k ; \mathbf{p} denotes the l -dimensional uncertain parameters involved in the nonlinear dynamic model represented by the symbol $\mathbf{f}(\cdot)$; \mathbf{z} denotes the m -dimensional measurements with their function represented by $\mathbf{h}(\cdot)$; \mathbf{v}_k is measurement noise with a known distribution $p(\mathbf{v}_k)$, which is usually assumed to follow a zero mean Gaussian PDF. For simplicity, the state and parameters are combined as $\mathbf{X} = [\mathbf{x}; \mathbf{p}]$ with the total dimensions of

$d = n + l$. In the Bayesian framework, one attempts to construct the posterior PDF $p(\mathbf{X}_k | \mathbf{z}_{1:k})$ of the state variables and parameters based on the information of the measurement and a prior PDF $p(\mathbf{X}_0)$. Then the state and parameters can be recovered from the posterior PDF. The formulation of Bayesian estimation will be introduced with details in Section 4.

3. Generalised Polynomial Chaos

3.1. Dynamical System Approximation by Generalised Polynomial Chaos

The gPC framework is used for efficient propagation of the probabilistic uncertainties in \mathbf{X}_0 . Generally two steps are involved in gPC algorithms: 1) the construction of a surrogate model of the system using the orthogonal polynomials and 2) the stochastic propagation of the initial uncertainties through evaluation of the surrogate model. In the context of gPC, the solution \mathbf{X} of Eq. 1 can be represented by an infinite series of orthogonal polynomials¹⁹⁾

$$\begin{aligned} \mathbf{X}(t, \boldsymbol{\xi}) = & c_0 \phi_0 + \sum_{i_1=1}^d c_{i_1} \phi_1(\xi_{i_1}) + \sum_{i_1=1}^d \sum_{i_2=1}^{i_1} c_{i_1 i_2} \phi_2(\xi_{i_1}, \xi_{i_2}) \\ & + \sum_{i_1=1}^d \sum_{i_2=1}^{i_1} \sum_{i_3=1}^{i_2} c_{i_1 i_2 i_3} \phi_3(\xi_{i_1}, \xi_{i_2}, \xi_{i_3}) + \dots, \end{aligned} \quad (3)$$

where ϕ_k is the generalised polynomial basis function of order k determined using the Wiener-Askey scheme²⁷⁾ based on the PDF of multidimensional random variables ξ_{i_j} ($i_j = 1, 2, \dots, d$) that typically represent the uncertainties in model parameters or initial and boundary conditions. The original PC expansion can only be assembled using Hermite polynomials, corresponding to standard Gaussian distribution of ξ_{i_j} . In the gPC context, however, the polynomial bases have been expanded into other types of functions. For instance, Legendre, Laguerre, and Jacobi are optimal selections for modelling the effects of random variables described by uniform, γ and β distributions, respectively, in order to achieve theoretical exponential convergence of the approximation. The families of PDFs and their corresponding families of orthogonal polynomials are summarised in Table 1.

Table 1. The families of distributions and corresponding families of orthogonal polynomials

Distribution $\boldsymbol{\xi}$	Polynomials $\Phi_k(\boldsymbol{\xi})$	Support
Gaussian	Hermite	(0, 1)
γ	Laguerre	[0, ∞)
β	Jacobi	[a , b]
Uniform	Legendre	[-1, 1]

The above expansions can be formulated in a concrete form via multidimensional basis functions, i.e.

$$\mathbf{X}(t, \boldsymbol{\xi}) = \sum_{\boldsymbol{\alpha} \in \mathbb{N}_0^d} C_{\boldsymbol{\alpha}} \Phi_{\boldsymbol{\alpha}}(\boldsymbol{\xi}) \quad (\mathbb{N}_0^d := \{(\alpha_1, \dots, \alpha_d) : \alpha_j \in \mathbb{N} \cup \{0\}\}), \quad (4)$$

where $\boldsymbol{\alpha} \in \mathbb{N}_0^d$ is a multidimensional index notation; $\Phi_k(\boldsymbol{\xi})$ denotes the multivariate basis function, which is defined as the tensor product of univariate polynomial basis functions with the

assumption that the random univariate variables ξ_i are independent, and identically distributed (IID)

$$\Phi_{\alpha}(\xi) = \Phi_{\alpha}(\xi_1, \xi_2, \dots, \xi_d) = \phi_{\alpha_1}^{(1)}(\xi_1)\phi_{\alpha_2}^{(2)}(\xi_2)\dots\phi_{\alpha_d}^{(d)}(\xi_d), \quad (5)$$

where $\alpha_d \in \mathbb{N}_0^1$ denotes the degree of the univariate polynomials $\phi_{\alpha_d}^{(d)}(\xi_d)$. In practical applications, the assembly of orthogonal polynomials in Eq. 4 needs to be truncated to a finite number. A standard truncation strategy corresponds to the total degree p of the polynomials and the dimensionality d of the random variables characterising the input uncertainties, hence the approximation of X with truncated gPC expansions is given as

$$\hat{X}(t, \xi) = \sum_{\alpha \in A_p^d} C_{\alpha} \Phi_{\alpha}(\xi) \quad (A_p^d = \{\alpha \in \mathbb{N}_0^d : \|\alpha\|_0 \leq d, \|\alpha\|_1 \leq p\}). \quad (6)$$

The total number of terms N in an expansion of total order p involving d random variables is given by

$$N = 1 + \sum_{s=1}^p \frac{1}{s!} \prod_{r=0}^{s-1} (d+r) = \frac{(p+d)!}{p!d!}. \quad (7)$$

Additionally, a hyperbolic truncation scheme based on q -norm is also used as an alternative, with the index sets given as

$$A_{p,q,d} = \{\alpha \in \mathbb{N}_0^d : \|\alpha\|_0 \leq d, \|\alpha\|_q \leq p\}, \quad (8)$$

where

$$\|\alpha\|_q = \left(\sum_{i=1}^d \alpha_i^q \right)^{1/q} \quad (0 < q \leq 1).$$

When $q = 1$, the hyperbolic truncation reduces to the standard truncation in Eq. 6. Due to the sparsity-of-effects principle that the low-order interactions of the polynomials take main effects, the hyperbolic truncation scheme leads to sparse gPC expansions,^{4,5)} which are more time efficient.

Substitution of the approximate solution \hat{X} into Eq. 1 results in errors, which are given by

$$e(N) = \dot{\hat{X}}(t, \xi) - f(t, \hat{X}, \xi) = \dot{\hat{X}}(t, \xi) - \sum_{\alpha \in A_p^d} C_{\alpha} \Phi_{\alpha}(\xi), \quad (9)$$

which indicates the truncation error depends on N in the standard truncation scheme and converges in the mean-square sense as N tends to infinity,²⁶⁾ i.e.

$$\lim_{N \rightarrow \infty} \langle e^2(N) \rangle = 0. \quad (10)$$

From above remarks, both the computational costs and approximation accuracy depend on the value of N . In practice, the dimensionality d of uncertainties is always deterministic with a specific system. Hence, the degree p needs to be decided in order to achieve a given error threshold but also to calculate the gPC coefficients efficiently.

3.2. Non-intrusive Approach to Solve gPC Coefficients

To build up the approximation of the solution \hat{X} , the polynomial coefficients need to be solved. The approaches can be categorised into two types: intrusive and non-intrusive approaches. In an intrusive approach, all the dependent random variables in the system equations are replaced with gPC expansions, which is straightforward but difficult to implement as it requires rewriting the whole programme of dynamic system in Eq. 1. Therefore, only non-intrusive approaches are considered in this work.

In this way, the system model is treated as a "black-box" so that the gPC coefficients are solved based on a set of simulation response evaluations. Generally two primary strategies have been proposed to calculate the polynomial coefficients non-intrusively in the literature, i.e., the spectral projection and the least-squares regression (LSR).^{2,8)} The LSR and its variant Least Angle Regression (LAR) are introduced in the work.

3.2.1. Least-squares Regression

The method of LSR solves the coefficients C_{α} by minimising the cost function²⁾

$$C_{\alpha} \approx \arg \min \frac{1}{M} \sum_{j=1}^M \left(X(t, \xi_j) - \sum_{\alpha \in A_p^d} C_{\alpha} \Phi_{\alpha}(\xi_j) \right)^2. \quad (11)$$

According to Eq. 11, the gPC expansions and corresponding coefficients can be written into a linear system

$$\begin{bmatrix} \Phi_{\alpha_1}(\xi_1) & \Phi_{\alpha_2}(\xi_1) & \dots & \Phi_{\alpha_N}(\xi_1) \\ \Phi_{\alpha_1}(\xi_2) & \Phi_{\alpha_2}(\xi_2) & \dots & \Phi_{\alpha_N}(\xi_2) \\ \vdots & \vdots & \ddots & \vdots \\ \Phi_{\alpha_1}(\xi_M) & \Phi_{\alpha_2}(\xi_M) & \dots & \Phi_{\alpha_N}(\xi_M) \end{bmatrix} \begin{bmatrix} \hat{C}_{\alpha_1}^T \\ \hat{C}_{\alpha_2}^T \\ \vdots \\ \hat{C}_{\alpha_M}^T \end{bmatrix} = \begin{bmatrix} X^T(t, \xi_1) \\ X^T(t, \xi_2) \\ \vdots \\ X^T(t, \xi_M) \end{bmatrix}. \quad (12)$$

The Eq. 12 can be formulated in a simple form

$$H\hat{C} = Y, \quad (13)$$

where H is a $M \times N$ matrix on the left hand side of Eq. 12, \hat{C} is the matrix of gPC coefficients, and Y is comprised of the surface response of the system model. The solution of the gPC coefficients can be given

$$\hat{C} = (H^T H)^{-1} H^T Y. \quad (14)$$

Figure 1 illustrates the degree of the N^{th} multivariate polynomial functions with respect to each univariate polynomial function. In this case, six inputs of position and velocity components are propagated using maximum 4th degree gPC. There are a total of 210 coefficients to be solved. The value of each coefficient is shown in Figure 2.

3.2.2. Least Angle Regression

LAR is proposed as an efficient procedure to select the polynomial basis functions that dominates the model response, in order to yield sparse gPC expansions for solution approximation.⁵⁾ The method of LAS solves the coefficients C_{α} by minimising the cost function

$$C_{\alpha} \approx \arg \min \frac{1}{M} \sum_{j=1}^M \left(X(t, \xi_j) - \sum_{\alpha \in A_p^d} C_{\alpha} \Phi_{\alpha}(\xi_j) \right)^2 + \lambda \sum_{\alpha \in A_p^d} |C_{\alpha}| \quad (15)$$

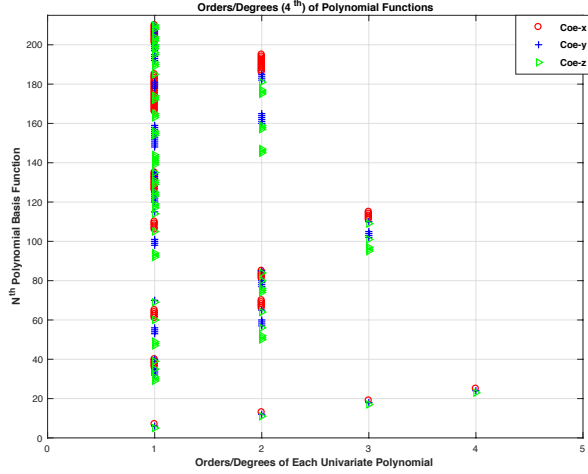


Fig. 1. Coefficients distributions

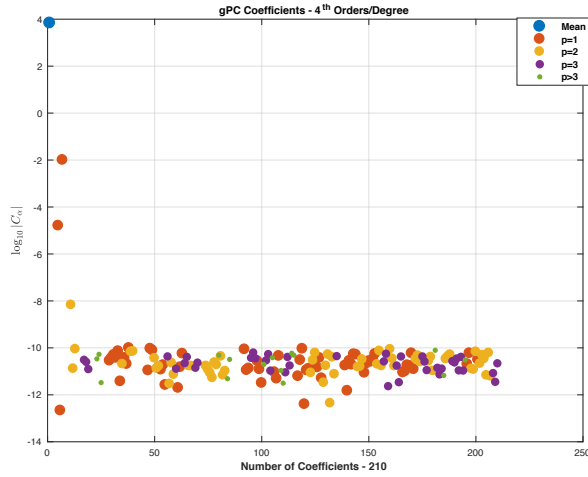


Fig. 2. gPC coefficients values

where λ is a positive scalar. An adaptive LAR procedure is detailed in [5].

For the following orbit determination demonstration, both LSR and LAR methods are used to solve gPC coefficients in the gPCPC filter, from which the best solutions are chosen.

4. Particle Filter

Sequential state estimation is the process of determining the states of a stochastic dynamical system epoch by epoch by incorporating the noisy measurements collected from the system's sensors with an imperfect dynamic model in the framework of various filtering techniques. The state typically evolves according to a Markov chain. Except for the linear case (with Gaussian noise), no closed-form solutions to the state estimation problem are known. A Markov process for the system function in Eq. 1 is assumed

$$p(\mathbf{X}_{t_0}|\mathbf{z}_0) = p(\mathbf{X}_{t_0}), \quad (16)$$

$$p(\mathbf{X}_{t_k}|\mathbf{X}_{t_{k-1}}, \mathbf{z}_{1:k-1}) = p(\mathbf{X}_{t_k}|\mathbf{X}_{t_{k-1}}), \quad (17)$$

where $p(\mathbf{X}_{t_0}|\mathbf{z}_0)$ is the the a priori PDF of the state vector.

In the measurement update step, the prior PDF is updated

with the new observation \mathbf{z}_k based on Bayes' theorem to obtain the posterior PDF

$$\underbrace{p(\mathbf{X}_{t_k}|\mathbf{z}_{1:k})}_{\text{Posterior}} = \frac{\underbrace{p(\mathbf{z}_k|\mathbf{X}_{t_k})}_{\text{Likelihood}} \underbrace{p(\mathbf{X}_{t_k}|\mathbf{z}_{1:k-1})}_{\text{Prior}}}{\underbrace{p(\mathbf{z}_k|\mathbf{z}_{1:k-1})}_{\text{Evidence}}}, \quad (18)$$

where $p(\mathbf{z}_k|\mathbf{X}_{t_k})$ is the measurement likelihood, which is obtained from the measurement model; the normalising denominator $p(\mathbf{z}_k|\mathbf{z}_{1:k-1})$ is given by

$$p(\mathbf{z}_k|\mathbf{z}_{1:k-1}) = \int p(\mathbf{z}_k|\mathbf{X}_{t_k})p(\mathbf{X}_{t_k}|\mathbf{z}_{1:k-1})d\mathbf{X}_{t_k}. \quad (19)$$

We can consider the update or filtering distribution as a weighting of the prediction distribution as in the full joint case above, i.e.

$$\underbrace{p(\mathbf{X}_{t_k}|\mathbf{z}_{1:k})}_{\text{Posterior}} = \underbrace{w_k}_{\text{Weight}} \underbrace{p(\mathbf{X}_{t_k}|\mathbf{z}_{1:k-1})}_{\text{Prior}}, \quad (20)$$

where in this case the weight is defined as

$$w_k = \frac{p(\mathbf{z}_k|\mathbf{X}_{t_k})}{p(\mathbf{z}_k|\mathbf{z}_{1:k-1})}. \quad (21)$$

In the time update step, $p(\mathbf{X}_{t_k}|\mathbf{z}_{1:k})$ is predicted to $p(\mathbf{X}_{t_{k+1}}|\mathbf{z}_{1:k})$ as shown in Eq. 22, which can be taken as a prior over \mathbf{X}_{t_k} before the most recent observation \mathbf{z}_k is available. $p(\mathbf{X}_{t_{k+1}}|\mathbf{X}_{t_k})$ is given by the system dynamics in Eq. 1.

$$p(\mathbf{X}_{t_{k+1}}|\mathbf{z}_{1:k}) = \int p(\mathbf{X}_{t_{k+1}}|\mathbf{X}_{t_k})p(\mathbf{X}_{t_k}|\mathbf{z}_{1:k})d\mathbf{X}_{t_k}. \quad (22)$$

Generally, the Eqs. 20 and 22 with the initial PDF given in Eq. 16 define a very conceptual solution of the sequential estimation problem. Analytical solutions for prediction and update steps in Eq. 20 - 22 can only be obtained with some specific assumptions. For instance, the Kalman filter deduced from the above rules has been proven to be an optimal filtering technique when the following two conditions are satisfied: 1) Both the system and measurement equations (Eqs. 1 and 2) are linear; 2) All the state and measurement noises ($p(\mathbf{X}_{t_0})$, $p(\mathbf{z}_k|\mathbf{X}_{t_k})$ and $p(\mathbf{X}_{t_k}|\mathbf{z}_k)$) follow Gaussian distributions. However, for nonlinear systems with non-Gaussian noises, it is impossible, in general, to estimate the state or/and parameters optimally and analytically. Attempts to force these problems into a linear and Gaussian framework by linearisation lead to EKF, SPKF and many variants. However, with nonlinearity and non-Gaussianity becoming much more severe, this type of approximation always results in divergence. In these cases, the PF turns out to be a good alternative.

The PF is a simulation-based sequential Monte Carlo method, which implements a sequential Bayesian filter by MCS without making any assumption on the PDF. The central idea of a PF is to represent the required PDF by a large number of IID samples (particles) $\mathbf{X}_{t_{k-1}}^{(i)}$ with associated weights $\omega_k^{(i)}$

$$p(\mathbf{X}_{t_k}|\mathbf{z}_{1:k}) \approx \sum_{i=1}^{N_s} \omega_k^{(i)} \delta(\mathbf{X}_{t_k} - \mathbf{X}_{t_k}^{(i)}), \quad (23)$$

where the i^{th} weight $\omega^{(i)}$ is normalised such that $\sum_{i=1}^{N_s} \omega^{(i)} = 1$; δ denotes the Delta function; N_s denotes the number of particles. As N_s becomes large, the estimated posterior PDF approaches

the real PDF. Then the state can be estimated using these particles and weights. Specifically, with the posterior PDF obtained based on the Bayes' rule, the state estimate can be solved by

$$\hat{\mathbf{X}}_{t_k} = \mathbf{E}_{p(\mathbf{X}_{t_k}|\mathbf{z}_{1:k})}[\mathbf{X}_{t_k}] := \int \mathbf{X}_{t_k} p(\mathbf{X}_{t_k}|\mathbf{z}_{1:k}) d\mathbf{X}_{t_k}. \quad (24)$$

The derivation of PFs is revisited here.^{1,10,11} According to the principle of *importance sampling*, the weights $\omega_k^{(i)}$ in Eq. 23 are defined as

$$\omega_k^{(i)} \propto \frac{p(\mathbf{X}_{t_0:t_k}^i|\mathbf{z}_{1:k})}{q(\mathbf{X}_{t_0:t_k}^i|\mathbf{z}_{1:k})}, \quad (25)$$

where $q(\mathbf{X}_{t_0:t_k}^i|\mathbf{z}_{1:k})$ is the importance distribution, from which the particles are drawn. Then an update equation for the weight can be derived by formulating $p(\mathbf{X}_{t_0:t_k}^i|\mathbf{z}_{1:k})$ using Bayes' rule

$$\omega_k^{(i)} = \omega_{k-1}^{(i)} \frac{\overbrace{p(\mathbf{z}_k|\mathbf{X}_{t_k}^i)}^{\text{Likelihood}} \overbrace{p(\mathbf{X}_{t_k}^i|\mathbf{X}_{t_{k-1}}^i)}^{\text{Transition}}}{q(\mathbf{X}_{t_0:t_k}^i|\mathbf{X}_{t_0:t_{k-1}}^i, \mathbf{z}_{1:k})}, \quad (26)$$

where the importance distribution is given by

$$q(\mathbf{X}_{t_0:t_k}^i|\mathbf{z}_{1:k}) = q(\mathbf{X}_{t_k}^i|\mathbf{X}_{t_0:t_{k-1}}^i, \mathbf{z}_k) q(\mathbf{X}_{t_0:t_{k-1}}^i|\mathbf{z}_{1:k-1}). \quad (27)$$

To save the memory of the filtering algorithm, the importance distribution is further simplified to be dependent solely on $\mathbf{X}_{t_{k-1}}^i$ and \mathbf{z}_k

$$q(\mathbf{X}_{t_k}^i|\mathbf{X}_{t_0:t_{k-1}}^i, \mathbf{z}_{1:k}) = q(\mathbf{X}_{t_k}^i|\mathbf{X}_{t_{k-1}}^i, \mathbf{z}_k). \quad (28)$$

This yields a modified weight expressed as

$$\omega_k^{(i)} \propto \omega_{k-1}^{(i)} \frac{p(\mathbf{z}_k|\mathbf{X}_{t_k}^i) p(\mathbf{X}_{t_k}^i|\mathbf{X}_{t_{k-1}}^i)}{q(\mathbf{X}_{t_k}^i|\mathbf{X}_{t_{k-1}}^i, \mathbf{z}_k)}. \quad (29)$$

The above equations present how the state estimate and its posterior PDF could be solved using sequential importance sampling technique.^{1,10} However, the particles meet with the degeneracy phenomenon. Since the prior PDF $p(\mathbf{X}_{t_k}^i|\mathbf{X}_{t_{k-1}}^i)$ is usually broader than the likelihood $p(\mathbf{z}_k|\mathbf{X}_{t_k}^i)$, the normalised weights tend to concentrate into one particle after a number of recursions.²⁰ The effective sample size is used to measure the sampling degeneracy, which is approximated by

$$\hat{N}_e = \frac{1}{\sum_{i=1}^{N_s} (\omega_k^{(i)})^2}. \quad (30)$$

Once the effective sample size \hat{N}_e is smaller than a threshold N_t , a resampling procedure is recommended to deal with the sampling degeneracy.^{1,16}

5. Generalised Polynomial Chaos Based Particle Filter

5.1. Isoprobabilistic Transformation

In the context of gPC, isoprobabilistic transformation^{2,6} is used to transform the random vector $\boldsymbol{\xi}$ that is not standardised into a set of reduced variables $\boldsymbol{\eta}$

$$\boldsymbol{\xi} = T(\boldsymbol{\eta}). \quad (31)$$

Depending on the distribution of each component of the variable $\boldsymbol{\xi}_i$, the associated reduced variable $\boldsymbol{\eta}_i$ can be represented by a Gaussian distribution, uniform distribution, etc. Then the

approximate state \mathbf{X} can be formulated as a function of the reduced variables $\boldsymbol{\eta}$

$$\mathbf{X}(t, \boldsymbol{\xi}) = \sum_{\alpha \in \mathbb{N}_0^d} C_\alpha \Phi_\alpha(T(\boldsymbol{\eta})) = \sum_{\alpha \in \mathbb{N}_0^d} \bar{C}_\alpha \Phi_\alpha(\boldsymbol{\eta}). \quad (32)$$

Note that the variables $\boldsymbol{\xi}$ are assumed independent. But isoprobabilistic transformation also can be used for correlated variables through, e.g., Nataf transformation.⁶

5.2. gPCPF Algorithm

Combining Eqs. 16, 22, 23, 29, the traditional bootstrap PF algorithm is summarised as below:^{1,10,11}

1. Initialisation at $k = 0$ for $i = 1, \dots, N_s$:
 - Generate N_s particles $\mathbf{X}_{t_0}^i$ from an initial distribution $p(\mathbf{X}_{t_0})$;
 - Set the normalised importance weights $\omega_0^{(i)} = 1/N_s$.

Repeat at each time $k \geq 1$ for $i = 1, \dots, N_s$:

2. Measurement update:

- The weights for the new sampling at current epoch can be calculated using Eq. 29;
- Normalise the weights

$$\omega_k^{(i)} = \frac{\omega_k^{*(i)}}{\sum_{i=1}^{N_s} \omega_k^{*(i)}}; \quad (33)$$

- The final posterior density is estimated using Eq. 23, and the state is updated

$$\hat{\mathbf{X}}_{t_k} = \sum_{i=1}^{N_s} \omega_k^{(i)} \mathbf{X}_{t_k}^i; \quad (34)$$

3. Resampling:

- Calculate the efficient sample size using Eq. 30;
- If $\hat{N}_e < N_t$, generate a new set of particles $\mathbf{X}_{t_k}^i$ according to Eq. 33, and let $\omega_k^{(i)} = 1/N_s$.

4. Time update:

- Generate predictions from the importance distribution

$$\mathbf{X}_{t_{k+1}}^i \sim q(\mathbf{X}_{t_{k+1}}^i|\mathbf{X}_{t_k}^i, \mathbf{z}_{k+1}). \quad (35)$$

In analogy to the traditional bootstrap PF algorithm, only the time update step needs to be substituted. Additionally, a common reasonable choice for the importance distribution $q(\mathbf{X}_{t_{k+1}}^i|\mathbf{X}_{t_k}^i, \mathbf{z}_{k+1})$ is the transition PDF $p(\mathbf{X}_{t_{k+1}}^i|\mathbf{X}_{t_k}^i)$ represented by the system function in Eq. 1,¹ which has been termed as the bootstrap PF. Hence, the weights involved in Eq. 29 can be rewritten as

$$\omega_k^{(i)} \propto \omega_{k-1}^{(i)} p(\mathbf{z}_k|\mathbf{X}_{t_k}^i). \quad (36)$$

The uncertainties involved in the transition PDF for the system function will be propagated by gPC expansions in Eq. 35. The gPCPF algorithm is illustrated in Figure 3.

6. Numerical Examples

Following previous discussion, we set up two orbit determination scenarios where nonlinear and non-Gaussian effects cannot be neglected. Both scenarios include an IGSO satellite with an orbital period of 24 hours. Range and range rate observations are simulated from different numbers of ground stations with different noises. No process noise is added for the current work.

Table 2. Satellite Initial Conditions in the ECI Coordinate System

x (m)	y (m)	z (m)	vx (m/s)	vy (m/s)	vz (m/s)
37334419.253	6402992.005	-13817229.687	-1259.3	2409.9	-1709.8

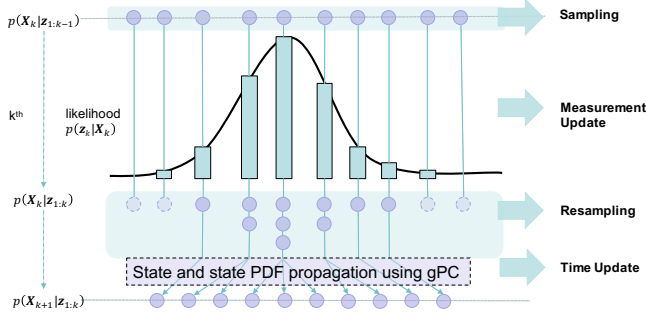


Fig. 3. gPCPF Algorithm Illustration

6.1. Scenario I

In the first scenario, only two-body motion is assumed for the space object. Three ground stations (see Figure 4 for the detailed information) are chosen for measurement simulation. An elevation mask of 20° with an interval of 600s is used for all the measurements. The initial state of the reference orbit is given in Table 2. A standard deviation value of 1m is given for each position component and that of 1mm/s is given for each velocity component in the initial covariance matrix.

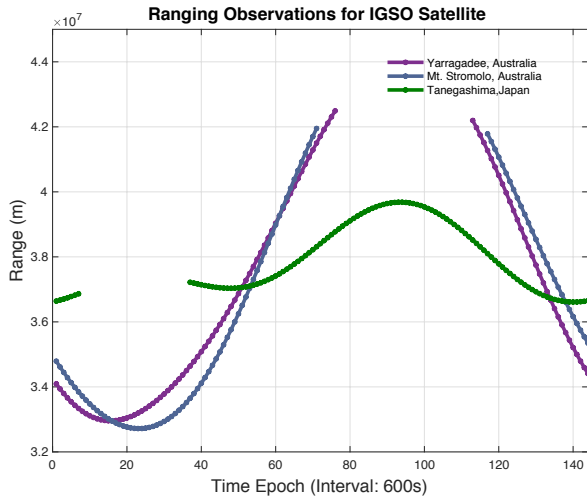


Fig. 4. Range Observations From Three Ground Stations (Elevation Mask: 20 Degrees)

To analyse the gPCPF performance with data outage, different numbers of ground station data are used. Statistical results of position and velocity estimation errors are given in the bar chart in Figure 5 and 6 in comparison with PF results. Generally speaking, gPCPF and PF share similar OD performance. With observations available from only one ground station, the 3D RMS (Root Mean Square) error of position estimates comes to approximately 3m with the largest contribution coming from the In-track direction.

Different observation standard deviation values are given for sensitivity analysis. As the range measurement 1σ grows from 1m to 100m, both position and velocity estimation accuracy and precision deteriorate using both PFs. The gPCPF generates similar results with the bootstrap PF. These results are shown in

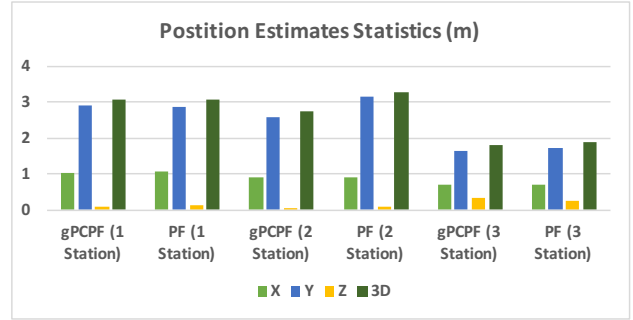


Fig. 5. Position Estimates Statistics (RMS Values) with Different Numbers of Ground Stations (gPCPF vs PF)

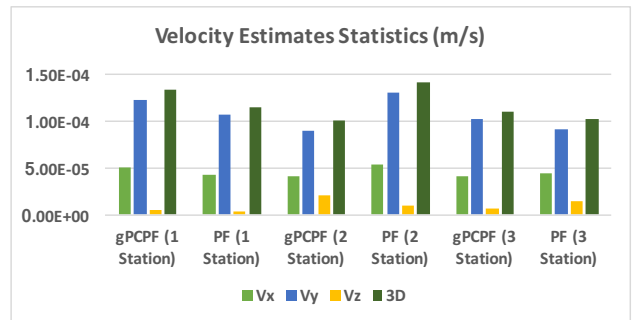


Fig. 6. Velocity Estimates Statistics (RMS Values) with Different Numbers of Ground Stations (gPCPF vs PF)

Figure 7 and Figure 8.

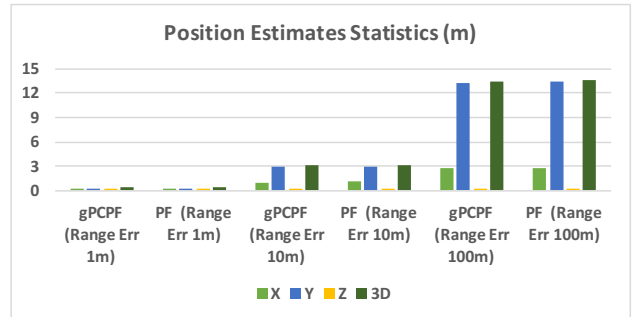


Fig. 7. Position Estimates Statistics (RMS Values) with Different Observation Errors (gPCPF vs PF)

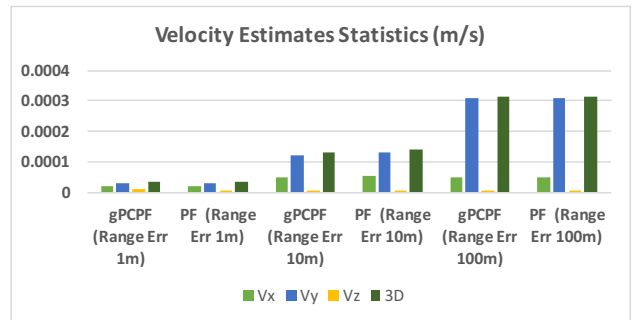


Fig. 8. Velocity Estimates Statistics (RMS Values) with Different Observation Errors (gPCPF vs PF)

Figure 9 and 10 plot the position and velocity errors in terms of RMS in the Radial, In-track and Cross-track frame using

gPCPF, respectively. Only one station's measurements are used with STD value of 10m and 1mm/s given to range and range rate measurements, respectively. It is obvious that the 3σ bounds get larger purely due to the orbit propagation without measurement correction in the middle of the process. When measurements become available again, the 3σ value stops increasing. Both position and velocity errors are all constrained by the 3σ bounds. The In-track components have largest errors in comparison with other two components.

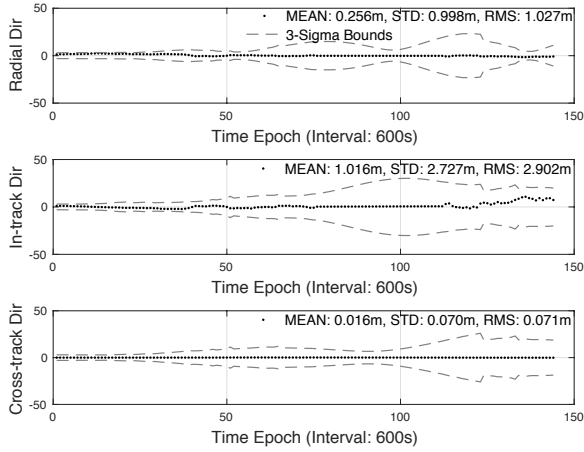


Fig. 9. Position Errors Using gPCPF with One Ground Station Observations

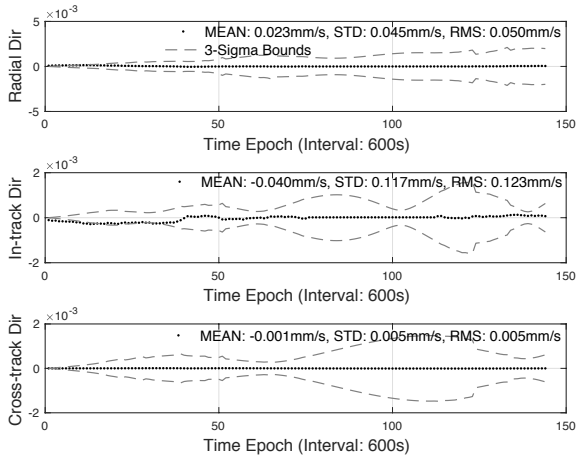


Fig. 10. Velocity Errors Using gPCPF with One Ground Station Observations

6.2. Scenario II

For space objects in the high altitude region (e.g., the geosynchronous orbit), the solar radiation pressure is one of the largest non-gravitational perturbations and can therefore have significant influence on their orbital dynamics. The acceleration of SRP is formulated as the following Eq. 37 for the cannonball assumption

$$\mathbf{a}_{\text{SRP}} = -\frac{P_{\text{SR}} C_{\text{R}} A_{\text{S}}}{m} \mathbf{r}_{\text{s}}, \quad (37)$$

where P_{SR} is the solar radiation pressure constant, C_{R} is the solar pressure parameter, A_{S} is the effective area facing the Sun, m

is the object mass and \mathbf{r}_{s} is the vector from the object to the Sun. In this scenario, the value of the ballistic coefficient, $B = \frac{C_{\text{R}} A_{\text{S}}}{m}$, is chosen to be 1.4, which is consistent with a HAMR object.⁽²²⁾ Only the Yarragadee station is used to generate observations hereafter, with $\sigma_{\rho} = 10\text{m}$ and $\sigma_{\dot{\rho}} = 1\text{mm/s}$ as standard deviation values for the range and range rate respectively.

To assess the effects of uncertain ballistic coefficient B on OD performance, the gPCPF is compared with the bootstrap PF in the following tests with different distributions (normal and uniform distributions) representing the uncertainty associated with B . A mean value of 1.4 and a variance value of 0.2 are specified for the normal distribution. An interval of [1.2 1.6] is given for the uniform distribution. Statistical values of the estimates, i.e., RMS, Mean and STD (Standard Deviation), are given in Figure 11 and Figure 12 for the position and velocity, respectively. It is clearly shown that gPCPF outperforms the bootstrap PF in terms of 3D error statistical analysis. By more accurately quantifying uncertainties of both initial state variables and dynamical parameters, gPCPF provides a better approach to predict covariance information forward in the time update step of the filter. Hence the gPCPF generates better OD solutions than the traditional bootstrap PF.

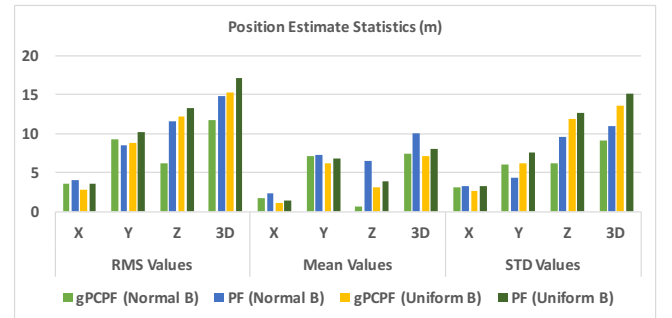


Fig. 11. Position Estimates Statistics with Different Distributions for Ballistic Coefficient B (gPCPF vs PF)

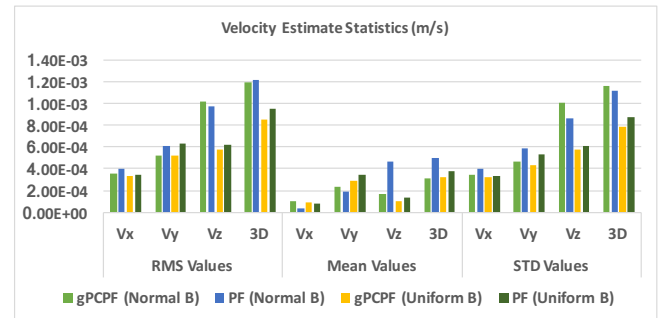


Fig. 12. Velocity Estimates Statistics with Different Distributions for Ballistic Coefficient B (gPCPF vs PF)

In Figure 13 and Figure 14, RMS values of position and velocity estimates using gPCPF are presented in the RIC coordinate system. All these estimates are duly constrained in the 3σ bounds. The 3D RMS errors reach 11.727m and around 1mm/s for the position and velocity respectively when the ballistic coefficient B is assumed as a normal distribution. While those values come to 15.255m and around 0.8mm/s with a uniform distributed B .

Finally, PF results are compared to EKF, UKF and GMUKF results in Figure 15 and Figure 16 for position and velocity,

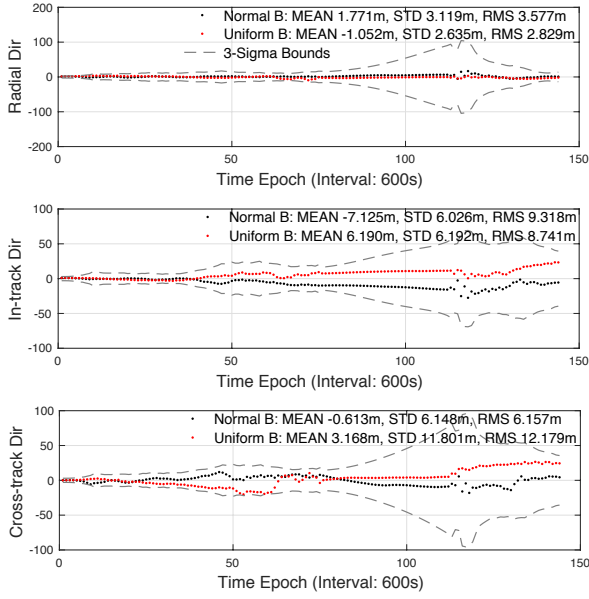


Fig. 13. Position Estimation Errors Using gPCPF with Different Distributions for Ballistic Coefficient B

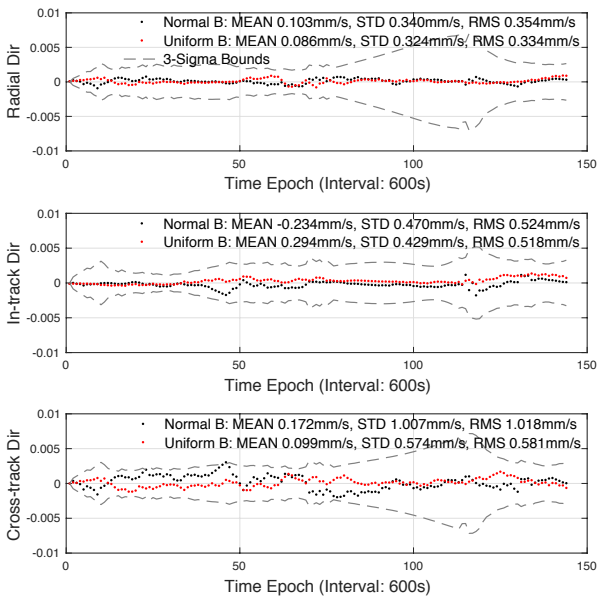


Fig. 14. Velocity Estimation Errors Using gPCPF with Different Distributions for Ballistic Coefficient B

respectively. Among them, GMUKF exploits a 5-component Gaussian mixture model (GMM) to approximate the initial multivariate Gaussian distribution. Afterwards, the number of GMM components is fixed but their weights are changing along the time. The ballistic coefficient is assumed to be normally distributed for the space object. Grey dash lines indicate the 3σ bounds calculated from the gPCPF in both figures. It is clearly shown that the Radial estimation outperforms the other two directions. Due to the geometry of the range measurements, it is more likely the imprecise orbit prediction with the uncertain SRP force can be corrected well in the Radial direction. When

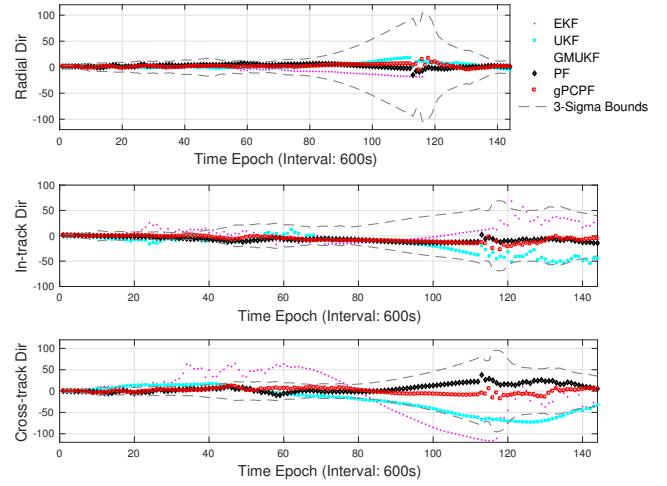


Fig. 15. Position Estimates Using Different Filters (EKF, UKF, GMUKF, PF and gPCPF)

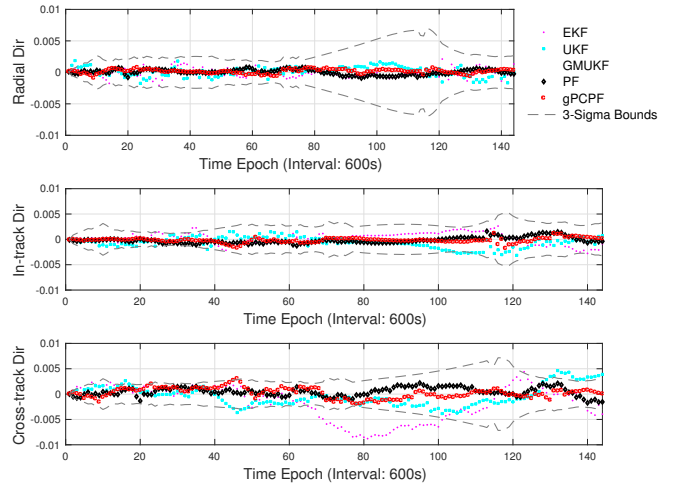


Fig. 16. Velocity Estimates Using Different Filters (EKF, UKF, GMUKF, PF and gPCPF)

the observation outage starts at the 76th epoch, the position estimates in all three directions for both EKF and UKF diverge significantly, even escaping out of the 3σ bounds. Both PF results also deteriorate but they are still constrained by the 3σ bounds. The velocity estimates turn out to be more stable than the position estimates. In the Cross-track direction, EKF estimates are much worse in comparison with the bootstrap PF and gPCPF, and have many unstable spikes. The state estimation performance by GMUKF are somewhat between EKF/UKF and PFs for both position and velocity components. Statistical values for position and velocity estimates using various filters are given in the Figure 17 and Figure 18. For position estimates, the proposed gPCPF has the best performance in terms of 3D RMS, Mean and STD values. For velocity estimates, gPCPF does not provide smallest 3D mean errors - larger than GMUKF, but it still generates good performance in terms of RMS and STD values.

Figure 19 presents the particles evolution in the gPCPF. It is clear the "Radial - In-track" plane of the orbit becomes non-Gaussian as time propagates. In particular, the In-track com-

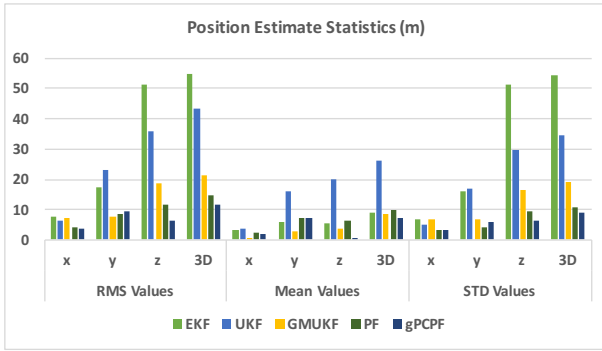


Fig. 17. Position Estimates Statistics Using Different Filters (EKF, UKF, GMUKF, PF and gPCPF)

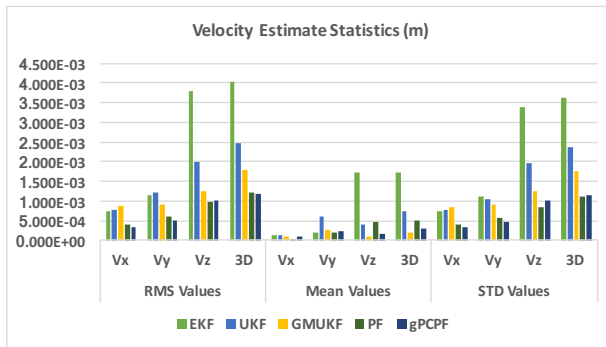


Fig. 18. Velocity Estimates Statistics Using Different Filters (EKF, UKF, GMUKF, PF and gPCPF)

ponent spreads out more significantly during the observation outage shown in the left-bottom subfigure. As observations become available again after the 113th epoch, the non-Gaussianity of the orbit becomes less severe as shown in the right-bottom subfigure.

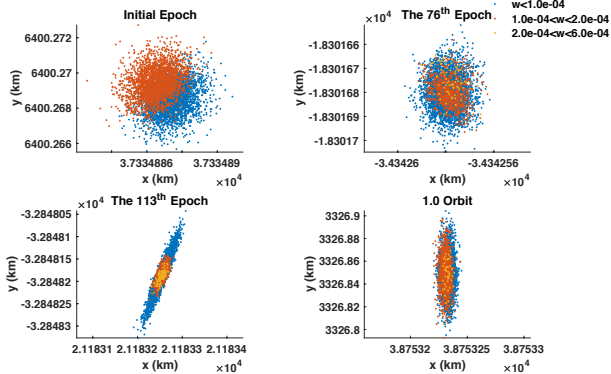


Fig. 19. Particle evolution in gPCPF

7. Conclusion

This paper presents a gPCPF based orbit determination approach for a high area-to-mass ratio space object in an inclined geosynchronous Earth orbit. In the framework of generalised polynomial chaos expansions, uncertainties associated with both initial state variables and dynamical parameters can be quantified very well. In this sense, the proposed gPCPF turns out to be more advantageous in comparison with the traditional bootstrap PF without significantly increasing computational burden. It is demonstrated that more accurate solutions

are generated by the gPCPF in the simulated orbit determination scenarios for the HAMR space object. Future work will focus on time efficiency analysis for the gPCPF with tuning gPC degrees, and more severe non-linear and non-Gaussian orbital scenarios (e.g., a highly elliptical orbit) will be studied.

Acknowledgments

The authors would like to acknowledge the support of the Cooperative Research Centre for Space Environment Management (SERC Limited) through the Australian Government's Cooperative Research Centre Programme. We wish to thank the Chair of Risk, Safety and Uncertainty Quantification of ETH Zürich for providing the UQLab software for polynomial chaos expansions based uncertainty quantification. We also appreciate the GMUKF codes shared by Dr Steve Gehly from SPACE Research Centre for comparison.

References

- Sanjeev Arulampalam, Simon Maskell, Neil Gordon, and Tim Clapp. A tutorial on particle filters for online nonlinear/non-gaussian bayesian tracking. *IEEE Transactions on Signal Processing*, 50(2):174–188, 2002.
- Marc Berveiller, Bruno Sudret, and Maurice Lemaire. Stochastic finite element: a non-intrusive approach by regression. *European Journal of Computational Mechanics*, 15(1–3):81–92, 2006.
- Emmanuel D. Blanchard, Adrian Sandu, and Corina Sandu. A polynomial chaos-based Kalman filter approach for parameter estimation of mechanical systems. *Journal of Dynamic Systems, Measurement, and Control*, 132(6):061404, 2010.
- Géraud Blatman and Bruno Sudret. An adaptive algorithm to build up sparse polynomial chaos expansions for stochastic finite element analysis. *Probabilistic Engineering Mechanics*, 25(2):183–197, 2010.
- Géraud Blatman and Bruno Sudret. Adaptive sparse polynomial chaos expansion based on least angle regression. *Journal of Computational Physics*, 230(6):2345–2367, April 2011.
- Sudret Bruno. Chapter 6 - Polynomial chaos expansions and stochastic finite-element methods. In Kok-Kwang Phoon and Jianye Ching, editors, *Risk and Reliability in Geotechnical Engineering*, pages 265–300. CRC Press, 2014.
- John L Crassidis. Sigma-point Kalman filtering for integrated GPS and inertial navigation. *Aerospace and Electronic Systems, IEEE Transactions on*, 42(2):750–756, 2006.
- Michael S. Eldred and John Burkardt. Comparison of non-intrusive polynomial chaos and stochastic collocation methods for uncertainty quantification. In *47th AIAA Aerospace Sciences Meeting including The New Horizons Forum and Aerospace Exposition, AIAA-2009-0976*, pages 1–20, January 2009.
- Arthur Gelb. *Applied optimal estimation*. MIT press, 1974.
- Neil J. Gordon, D. J. Salmond, and A. F. M. Smith. Novel approach to nonlinear/non-Gaussian Bayesian state estimation. *IEE Proceedings F - Radar and Signal Processing*, 140(2):107–113, 1993.
- Fredrik Gustafsson. Particle filter theory and practice with positioning applications. *IEEE Aerospace and Electronic Systems Magazine*, 25(7):53–82, July 2010.
- Kazufumi Ito and Kaiqi Xiong. Gaussian filters for nonlinear filtering problems. *IEEE Transactions on Automatic Control*, 45(5):910–927, 2000.
- Brandon A. Jones, Alireza Doostan, and George H. Born. Nonlinear propagation of orbit uncertainty using non-intrusive polynomial chaos. *Journal of Guidance, Control, and Dynamics*, 36(2):430–444, 2013.
- Simon Julier, Jeffrey Uhlmann, and Hugh F. Durrant-Whyte. A new method for the nonlinear transformation of means and covariances

- in filters and estimators. *IEEE Transactions on Automatic Control*, 45(3):477–482, Mar 2000.
- 15) Rudolph Emil Kalman. A new approach to linear filtering and prediction problems. *Journal of Basic Engineering*, 82(1):35–45, 1960.
 - 16) Deok-Jin Lee. Nonlinear Bayesian filtering with applications to estimation and navigation, 2005. Copyright - Database copyright ProQuest LLC; ProQuest does not claim copyright in the individual underlying works; Last updated - 2016-03-14.
 - 17) Jia Li and Dongbin Xiu. A generalized polynomial chaos based ensemble Kalman filter with high accuracy. *Journal of Computational Physics*, 228(15):5454–5469, August 2009.
 - 18) Reza Madankan, Puneet Singla, Tarunraj Singh, and Peter D. Scott. Polynomial-chaos-based Bayesian approach for state and parameter estimations. *Journal of Guidance, Control, and Dynamics*, 36(4):1058–1074, July 2013.
 - 19) Oliver Le Maître and Omar M. Knio. Chapter 2 - Spectral Expansions. In Oliver Le Maître and Omar M. Knio, editors, *Spectral Methods for Uncertainty Quantification: With Applications to Computational Fluid Dynamics*, Scientific Computation, pages 17 – 44. Springer Netherlands, 2010.
 - 20) Alinda Mashiku, James L Garrison, and J Russell Carpenter. Statistical orbit determination using the particle filter for incorporating non-Gaussian uncertainties. In *AIAA/AAS Astrodynamics Specialist Conference*, pages 13–16. American Institute of Aeronautics and Astronautics, 2012.
 - 21) Magnus Nørsgaard, Niels K Poulsen, and Ole Ravn. New developments in state estimation for nonlinear systems. *Automatica*, 36(11):1627–1638, 2000.
 - 22) Thomas Schildknecht, R. Musci, and Tim Flohrer. Properties of the high area-to-mass ratio space debris population at high altitudes. *Advances in Space Research*, 41(7):1039 – 1045, 2008.
 - 23) Vivek Vittaldev, Ryan P Russell, and Richard Linares. Spacecraft uncertainty propagation using Gaussian mixture models and polynomial chaos expansions. *Journal of Guidance, Control, and Dynamics*, pages 2615–2626, 2016.
 - 24) Greg Welch and Gary Bishop. An introduction to the Kalman filter. Department of Computer Science, University of North Carolina, 2006.
 - 25) Norbert Wiener. The homogeneous chaos. *American Journal of Mathematics*, 60(4):897–936, 1938.
 - 26) Dongbin Xiu. *Numerical methods for stochastic computations: a spectral method approach*. Princeton University Press, 2010.
 - 27) Dongbin Xiu and George Em Karniadakis. The Wiener–Askey polynomial chaos for stochastic differential equations. *SIAM journal on scientific computing*, 24(2):619–644, January 2002.
 - 28) Yang Yang, Han Cai, and Kefei Zhang. Schmidt-Kalman filter with polynomial chaos expansion for orbit determination of space objects. In *Advanced Maui Optical and Space Surveillance Technologies Conference*, 2016.